

# Buckling analysis of nano composite sandwich Euler-Bernoulli beam considering porosity distribution on elastic foundation using DQM

Mohammad Mehdi Nejadi and Mehdi Mohammadimehr\*

Department of Solid Mechanics, Faculty of Mechanical Engineering, University of Kashan, Kashan, Iran

(Received April 13, 2019, Revised June 15, 2019, Accepted September 28, 2019)

**Abstract.** In the present study, buckling analysis of sandwich composite (carbon nanotube reinforced composite and fiber reinforced composite) Euler-Bernoulli beam in two configurations (core and layers material), three laminates (combination of different angles) and two models (relative thickness of core according to peripheral layers) using differential quadrature method (DQM) is studied. Also, the effects of porosity coefficient and different types of porosity distribution on critical buckling load are discussed. Using sandwich beam, it shows a considerable enhancement in the critical buckling load when compared to ordinary composite. Actually, resistance against buckling in sandwich beam is between two to four times more. It is also showed the critical buckling loads of laminate 1 and 3 are significantly larger than the results of laminate 2. When Configuration 2 is used, the critical buckling load rises about 3 percent in laminate 1 and 3 compared to the results of configuration 1. The amount of enhancement for laminate 3 is about 17 percent. It is also demonstrated that the influence of the core height (thickness) in the case of lower carbon volume fractions is ignorable. Even though, when volume fraction of fiber increases, differences grow smoothly. It should be noticed the amount of decline has inverse relationship with the beam aspect ratio. Among three porosity patterns investigated, beam with the distribution of porosity Type 2 (downward parabolic) has the maximum critical buckling load. At the end, the first three modes of buckling will be demonstrated to investigate the effect of spring constants.

**Keywords:** nano composite sandwich Euler-Bernoulli beam; buckling analysis; various porosity distributions; DQM

## 1. Introduction

Porous materials are widely used in structural design of wide number of fields and industries including transportation, aerospace, energy and construction according to their low specific weight, and increased machinability. Carbon nanotube (CNT) has been accepted as an excellent material for the reinforcement of polymer composites due to their high elastic modulus and low density (Esawi and Farag 2007). CNTs are also recently combined with porous materials to be used in various areas specially composites (Gui *et al.* 2011). Porous materials with functional properties have some similarities with the functionally graded materials. The porosity can cause a smooth or rough change in mechanical properties depends on some parameters such as porosity distributions and volume fraction of composite.

During the last several years, the problem of buckling of the porous materials with varying properties has been discussed by many authors. Thermal buckling behavior of functionally graded carbon nanotube-reinforced composite plates was investigated by Shen and Zhang (2010). The buckling analysis of thin functionally graded (FG) rectangular plates based on the classical or first order shear deformation theory (FSDT) under various loads were

discussed by Mohammadi *et al.* (2010). Jabbari *et al.* (2013, 2014) examined porosity distribution influence on buckling characteristics of plates. Buckling of metal foam porous beams using a shear deformation beam model was studied by Chen *et al.* (2015). Elastic properties were evaluated for different volume fractions along the material principal directions using finite element method (FEM) by Sudheer *et al.* (2015).

The high order buckling of two types of sandwich beams including AL-foam or PVC-foam flexible core and CNTs reinforced nanocomposite face sheets were investigated by Mohammadimehr and Shahedi (2017). Cong *et al.* (2018), Duc *et al.* (2016, 2017b, and 2018b) analyzed plate behavior based on higher-order shear deformation theory (HSDT) on elastic foundations under different loadings. A finite element method was proposed by Zghal *et al.* (2017) for linear static analysis of FG carbon nanotube-reinforced composite. The results are illustrated by three numerical examples in order to outline the performance. Postbuckling analysis of nonhomogeneous nano plates considering even and uneven distributions of porosity with the usage of nonpolynomial shear deformation theory was demonstrated by Barati and Zenkour (2018). The nonlocal critical buckling loads in relation to buckling mode number, and aspect ratio, in the presence and absence of an elastic medium, were examined by Chemi *et al.* (2018). Nonlinear dynamic behavior of imperfect functionally graded structures were investigated in many different shapes such as: curved shallow (Duc *et al.* 2016), cylindrical shell (Duc *et al.* 2016, 2017a, Rostami *et*

---

\*Corresponding author, Associate Professor,  
E-mail: mmohammadimehr@kashanu.ac.ir

*al.* 2019), conical (Duc *et al.* 2018a), and spherical (Anh *et al.* 2015) theories. Mohammadimehr *et al.* (2017) presented nonlinear vibration analysis of FG-CNTRC sandwich Timoshenko beam based on modified couple stress theory subjected to longitudinal magnetic field using generalized differential quadrature method. Mohammadimehr and Mohammadi Hooyeh (2018) depicted vibration analysis of magneto-electro-elastic timoshenko micro beam using surface stress effect and modified strain gradient theory under moving nano-particle. Shahedi and Mohammadimehr (2019) showed vibration analysis of rotating fully-bonded and delaminated sandwich beam with CNTRC face sheets and AL-foam flexible core in thermal and moisture environments. Amini *et al.* (2019) presented active control to reduce the vibration amplitude of the solar honeycomb sandwich panels with carbon nanotube reinforced composite (CNTRC) facesheets using piezoelectric patch sensor and actuator. Mohammadimehr *et al.* (2019) considered free vibration and buckling analyses of functionally graded annular thin sector plate in-plane loads using GDQM. Alimirzaei *et al.* (2019) illustrated nonlinear analysis of viscoelastic micro-composite beam with geometrical imperfection using FEM: MSGT electro-magneto-elastic bending, buckling and vibration solutions.

Ghorbanpour Arani *et al.* (2016) presented surface stress and agglomeration effects on nonlocal biaxial buckling polymeric nanocomposite plate reinforced by CNT using various approaches. Critical buckling load of a single-walled carbon nanotube (SWCNT) embedded in Kerr's medium was studied by Tayeb Bensattalah *et al.* (2018). Responses of the double-walled carbon nanotubes(DWCNTs) for various boundary conditions were discussed by Kumar (2018). The influences of volume percent of SWCNTs, geometrical parameters, elastic foundation and boundary conditions on the buckling of column were investigated by Arani and Kolahchi (2016).

Metallic copper nanoparticles were synthesised by reduction of copper ions in aqueous solution, and metal-metal bonding by using the nanoparticles was studied by Kobayashi *et al.* (2017). Interactions between pre-formed metal nanoparticles were studied by Low and Shon (2018).

In the present paper, the buckling analysis of sandwich composite beam consists of carbon nanotube reinforced composite (CNTRC) and fiber reinforced composite (FRC) beam in two different configurations, three various laminates and two models using differential quadrature method (DQM) will be analyzed. Moreover, influences of porosity coefficient and porosity distribution types on critical buckling load will be discussed. At the end, the first three modes of buckling for different spring constants will be demonstrated.

## 2. Problem statement

The sandwich composite beam composed of a core and two layers in the top and bottom is resting on shear layer and Winkler spring with two different configurations (Fig. 1(a)). In Configuration 1, the core is made of carbon nanotube reinforced composite (CNTRC) and the top and bottom layers are made of fibre reinforced composite (FRC). In configuration 2, the material of core is replaced with the material of top and bottom layers and the other way around. For discussing the influence of angles on the buckling load, three laminates are defined in the present paper as follows:

- Laminate 1:

$$\theta_{1t} = 0, \theta_{2t} = 90, \theta_{1c} = 0, \theta_{2c} = 45, \theta_{3c} = 90$$

- Laminate 2:

$$\theta_{1t} = 45, \theta_{2t} = -45, \theta_{1c} = 45, \theta_{2c} = -45, \theta_{3c} = 45$$

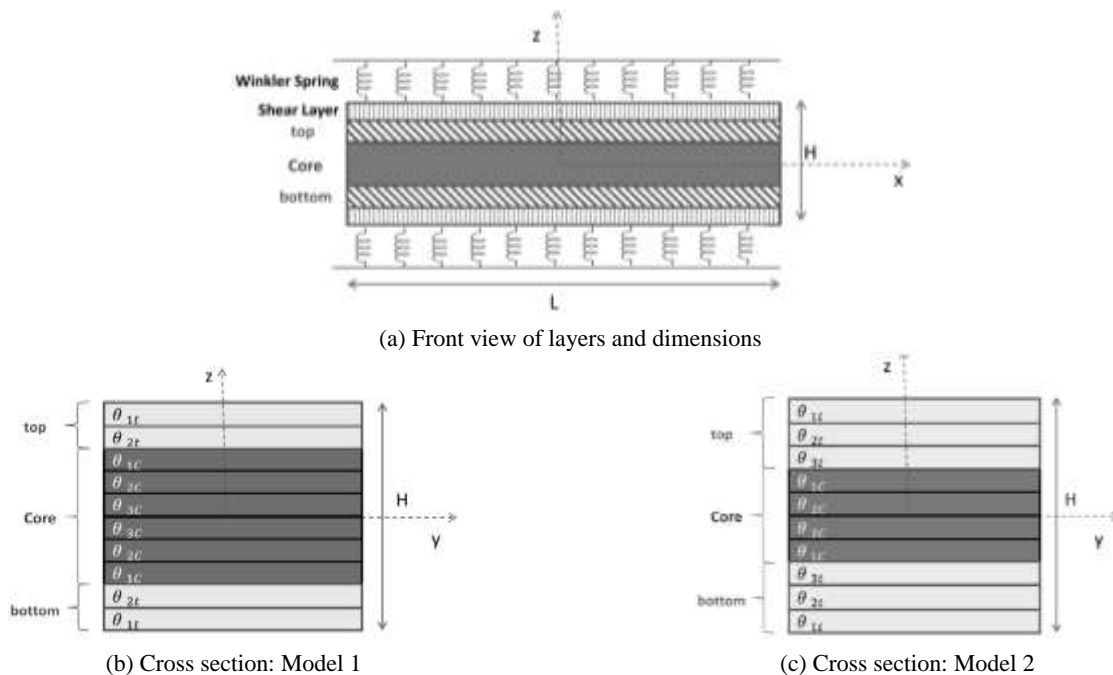


Fig. 1 Sandwich composite beam resting on elastic foundations

- Laminate 3:

$$\theta_{1t} = 0, \theta_{2t} = 90, \theta_{1c} = 0, \theta_{2c} = 60, \theta_{3c} = 75$$

In addition, two different models are investigated. In Model 1, the height of each peripheral layer is one-third of core height (Fig. 1(b)). Even though, in Model 2, the height of top or bottom layer is three-fourth of core height (Fig. 1(c)). All results in the present paper are obtained with Model 1 if it is not mentioned otherwise.

Governing equation for the buckling of Euler–Bernoulli composite beam is defined in Eq. (1a) (Tang *et al.* 2018).

$$\frac{d^4 w}{dx^4} + \beta \frac{d^2 w}{dx^2} + \gamma w = 0 \quad (1a)$$

$$\beta = \frac{Pcr}{E_{ef}I} \quad (1b)$$

$$\gamma = \frac{Kl^2}{E_{ef}I} \quad (1c)$$

where  $\beta$  and  $\gamma$  represent the stiffness parameter of Winkler foundation (Eq. (1b)) and shear modulus of Pasternak foundation (Eq. (1c)) (Mohammadimehr *et al.* 2010), respectively.  $Pcr$  is critical buckling load,  $I$  is moment of inertia for the cross section,  $K$  is shear spring constant and  $E_{ef}$  is effective modulus of elasticity which can be presented by the Eq. (2).

$$E_{ef} = \frac{8}{h^3} \sum_{j=1}^{m/2} (E_x)_j (z_j^3 - z_{j-1}^3) \quad (2)$$

where  $m$  is the number of layers,  $h$  is the height of the beam,  $z$  is distance between the outer plane of  $j$ th layer and the neutral axis.

Dimensionless critical buckling load can be obtained by Eq. (3) (Kumar and Srinivas 2017)

$$N_{cr} = \frac{P_{cr}}{A_{110}} \quad (3)$$

where  $A_{11}$  expressed by Eq. (4) is extensional stiffness of beam and  $A_{110}$  represents  $A_{11}$  for the beam made of pure matrix.

$$A_{11} = \sum_{k=1}^n \int_{h_{k-1}}^{h_k} (\bar{Q}_{11})_k dz \quad (4)$$

In the mentioned equation,  $h_k$  and  $h_{k-1}$  are the  $z$  values for the top and bottom and  $\bar{Q}_{11}$  is the transformed elastic constant of the  $k$ th layer could be calculated by Eq. (5)

$$\bar{Q}_{11} = Q_{11}c^4 + Q_{22}s^4 + (2Q_{12} + 4Q_{33})s^2c^2 \quad (5)$$

where

$$s = \sin\theta, \quad c = \cos\theta$$

$$Q_{11} = \frac{E_1}{1 - \nu_{12}\nu_{21}}, \quad Q_{22} = \frac{E_2}{1 - \nu_{12}\nu_{21}}$$

$$Q_{12} = \frac{\nu_{12}E_2}{1 - \nu_{12}\nu_{21}}, \quad Q_{33} = G_{12}$$

### 3. Solving method

To solve the Eq. (1) by Differential Quadrature Method (DQM), the first-order, the second-order, the third-order and the fourth derivatives of any arbitrary function in arbitrary point can be approximated in all intervals as follows in Eq. (6)

$$\frac{d^r f}{dx^r} (x = x_i) = \sum_{k=1}^n A^r_{ik} f(x_k) \quad (6)$$

where  $A^r$  is weighted coefficient matrices which are defined by Eqs. (7), (8) and (9).

$$A_{ij}^{(1)} = \frac{\prod_{m \neq i, j} (x_i - x_m)}{\prod_{m \neq j} (x_j - x_m)} \quad (i = j = 1, 2, 3, \dots, N; i \neq j) \quad (7)$$

$$A_{ij}^{(1)} = \sum_{m=1}^N \frac{1}{(x_i - x_m)} \quad (i = j = 1, 2, 3, \dots, N) \quad (8)$$

$$A^r = A^{(r-1)} A^r \quad 2 \leq r \leq N - 1 \quad (9)$$

Chebyshev points which are well-recognized set of the grid points for interval  $[0, L]$  are presented by Eq. (10).

For more details and deep understanding the DQ method, the review paper of Tornabene *et al.* (2015) is strongly advised.

### 4. Material properties

Mechanical properties of nanocomposite beam made of CNT reinforced polymer can be estimated using extended rule of mixture as follows in Eqs. (11) to (14) (Attanasakulpong and Ungbhakorn 2013, Mohammadimehr and Alimirzaei 2016)

$$E_{11} = \eta_1 V_{CNT} E_{11}^{CNT} + V_m E^m \quad (10)$$

$$\frac{\eta_2}{E_{22}} = \frac{V_{CNT}}{E_{22}^{CNT}} + \frac{V_m}{E^m} \quad (11)$$

$$\frac{\eta_3}{G_{12}} = \frac{V_{CNT}}{G_{12}^{CNT}} + \frac{V_m}{G^m} \quad (12)$$

$$\nu_{12} = V_{CNT} \nu_{12}^{CNT} + V_m \nu^m \quad (13)$$

where  $E_{11}^{CNT}$  and  $E_{22}^{CNT}$  represent the Young's modulus of the carbon nano tube parallel and perpendicular to the beam and considered to be 600 and 10 GPa, respectively.  $G_{12}^{CNT}$  and  $\nu_{12}^{CNT}$  which are the shear modulus and Poisson's ratio of carbon nanotube equal to 17.2 GPa and 0.19, respectively. Also  $E^m = 2.5 \text{ GPa}$  and  $G^m = 0.933 \text{ GPa}$

Table 1 Mechanical properties of CNTRC based on extended rule of mixture

$V_{CNT}$	$\eta_1$	$\eta_2$	$\eta_3$	$E_{11}$ (GPa)	$E_{22}$ (GPa)	$G_{12}$ (GPa)	$\nu_{12}$
0.12	1.2833	1.0556	1.0556	2.3626	2.9000	1.1110	3.2218
0.17	1.3414	1.7101	1.7101	2.3157	4.9000	1.9012	5.4437
0.28	1.3238	1.7380	1.7380	2.1913	5.5000	2.2056	6.1103

Table 2 Comparing the critical buckling loads of CNTRC with the results of Yas and Samadi (2012). Aspect ratio of the beam is 15

$(\beta, \gamma)$	B.C's	$V_{CNT}$	$\bar{N}_{Cr}$ (Present study)	$\bar{N}_{Cr}$ Yas and Samadi (2012)	Difference (%)
(0,0)	CF	0.12	0.03147	0.031234	0.74
	CF	0.17	0.04620	0.046318	-0.25
	CF	0.28	0.07458	0.072178	3.32
(0.1,0.02)	HH	0.12	0.12625	0.128729	-1.92
	HH	0.17	0.18538	0.180692	2.59
	HH	0.28	0.07642	0.083912	-8.92

and  $\nu^m = 0.34$  indicate the corresponding properties for the PMMA matrix. Efficiency factors are denoted by  $\eta_1$ ,  $\eta_2$  and  $\eta_3$  which are related to the nano-scale size effect (Kumar and Srinivas 2017). The mentioned properties of composite are calculated in Table 1.

The mechanical properties of composite made of carbon fiber reinforced polymer could be obtained by rule of mixture expressed by Eqs (15) to (18) (Sudheer *et al.* 2015). The parameters are the same which were described for the CNTs and the superscript f and m indicate the properties of fiber and matrix, respectively (Mohammadimehr *et al.* 2018).

$$E_{11} = V_f E_{11}^f + V_m E^m \quad (14)$$

$$\frac{1}{E_{22}} = \frac{V_f}{E_{22}^f} + \frac{V_m}{E^m} \quad (15)$$

$$\frac{1}{G_{12}} = \frac{V_f}{G_{12}^f} + \frac{V_m}{G^m} \quad (16)$$

$$\nu_{12} = V_f \nu_{12}^f + V_m \nu^m \quad (17)$$

Elastic properties of carbon fiber (Kumar and Srinivas 2017) are represented as follows:  $E_{11}^f = 600 \text{ GPa}$ ,  $E_{22}^f = 14 \text{ GPa}$ ,  $G_{12}^f = 9 \text{ GPa}$ ,  $\nu_{12}^f = 0.2$  and volume fractions of fibers are considered to be 0.4.

## 5. Results and discussion

Dimensionless critical buckling load of CNTRC with and without elastic foundations is presented in Table 2. It should be mentioned  $\beta$  and  $\gamma$  represent Winkler and shear spring constants, respectively. The buckling loads are compared with the results of Yas and Samadi (2012) for three volume fraction of carbon nanotube and two different

boundary conditions (Clamped-Free and Hinged-Hinged). As can be seen, the results are in good agreements.

Dimensionless critical buckling load for CNTRC and sandwich (CNTRC+FRC) beam against aspect ratio of beam for three CNT volume fractions are compared in Fig. 2. The clamped-free (CF) boundary condition is applied and the laminate 1 (as described in section Problem) is chosen. Winkler and shear spring constants are considered to be 0.1 and 0.02, respectively. As can be seen, there is a significant increment in the amount of buckling load by using sandwich beam. For instance, it is shown that resistancy against buckling in sandwich beam is almost four times more than CNTRC beam. Although with the increasing of CNT volume fraction, the influence of sandwich beams decreases, it is still noticeable.

For adding porosity consideration, the elastic properties of matrix of composite are assumed to vary by two types of porosity distribution across the height.

Porosity distribution, Type 1 is presented by Eqs. (19) to (21) as described in Jabbari *et al.* (2016).

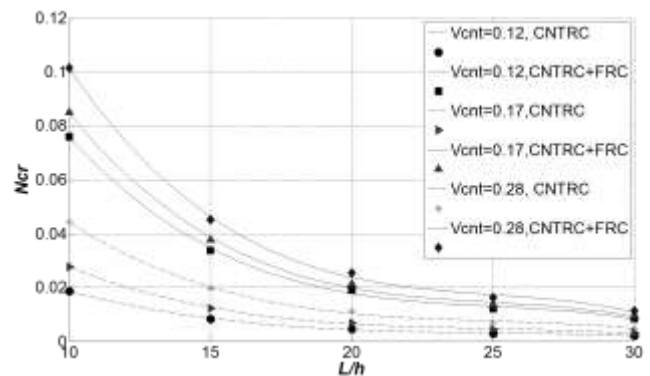


Fig. 2 Comparison of buckling load for CNTRC and sandwich (CNTRC+FRC) beam against aspect ratio of beam for three CNT volume fractions

$$E(z) = E_0 \left[ 1 - e_1 \cos \left( \left( \frac{\pi}{h} \right) z \right) \right] \quad (18)$$

$$G(z) = G_0 \left[ 1 - e_1 \cos \left( \left( \frac{\pi}{h} \right) z \right) \right] \quad (19)$$

$$\nu(z) = \nu_0 \left[ 1 - e_1 \cos \left( \left( \frac{\pi}{h} \right) z \right) \right] \quad (20)$$

where  $E_1$  and  $E_0$  are the Young's modulus of elasticity,  $G_1$  and  $G_0$  represent shear modulus,  $\nu_1$  and  $\nu_0$  denote Poisson's ratio at the bottom and the top of beam, respectively. Coefficient of beam porosity represented by  $e_1$  is obtained by Eq. (22).

$$e_1 = 1 - \frac{E_1}{E_0} \quad (21)$$

According to Eq. (22), in case porosity coefficient 0, there is no porosity and the bottom and top of the layer have the same Young's modulus; while when the porosity

coefficient is equal to 1, the maximum porosity occurs between two layers.

Porosity distribution, Type 2 is presented by Eqs. (23) to (25).

$$E(z) = E_0 \left[ 1 - e_1 \left( 1 - \cos \left( \left( \frac{\pi}{h} \right) z \right) \right) \right] \quad (22)$$

$$G(z) = G_0 \left[ 1 - e_1 \left( 1 - \cos \left( \left( \frac{\pi}{h} \right) z \right) \right) \right] \quad (23)$$

$$\nu(z) = \nu_0 \left[ 1 - e_1 \left( 1 - \cos \left( \left( \frac{\pi}{h} \right) z \right) \right) \right] \quad (24)$$

Fig. 2 shows the comparison of buckling load for CNTRC and sandwich (CNTRC+FRC) beam against aspect ratio of beam for three CNT volume fractions. With the increasing of carbon nanotube volume fraction, the critical buckling load of sandwich beams increases.

Porosity distribution, Type 3 is denoted by Eqs. (26) to (28).

Table 3 Critical buckling load for three famous volume fractions of carbon nanotube and Clamped-Free boundary conditions for Configuration 1

Configuration 1	L/H	$e_1$	$V_{CNT}$	$\bar{N}_{Cr}$	$V_{CNT}$	$\bar{N}_{Cr}$	$V_{CNT}$	$\bar{N}_{Cr}$
Laminate 1	10	0	0.12	0.072860521	0.17	0.081493337	0.28	0.098120809
		0.5		0.072856263		0.081488739		0.098116128
		1		0.072852005		0.081484141		0.098111445
	20	0	0.01821513	0.020373334	0.024530202			
		0.5	0.018214066	0.020372185	0.024529032			
		1	0.018213001	0.020371035	0.024527861			
	30	0	0.008095613	0.009054815	0.010902312			
		0.5	0.00809514	0.009054304	0.010901792			
		1	0.008094667	0.009053793	0.010901272			
Laminate 2	10	0	0.12	3.49626E-05	0.17	3.91155E-05	0.28	4.08199E-05
		0.5		2.38376E-05		2.66689E-05		2.78311E-05
		1		0.000012709		1.42183E-05		1.4838E-05
	20	0	8.74065E-06	9.77887E-06	1.0205E-05			
		0.5	5.95941E-06	6.66722E-06	6.95777E-06			
		1	3.17724E-06	3.55458E-06	3.70951E-06			
	30	0	3.88473E-06	4.34616E-06	4.53554E-06			
		0.5	2.64863E-06	2.96321E-06	3.09234E-06			
		1	1.41211E-06	1.57981E-06	1.64867E-06			
Laminate 3	10	0	0.12	0.072860095	0.17	0.081492605	0.28	0.098119951
		0.5		0.072855973		0.08148824		0.098115543
		1		0.072851850		0.081483875		0.098111133
	20	0	0.018215024	0.020373151	0.024529988			
		0.5	0.018213993	0.02037206	0.024528886			
		1	0.018212962	0.020370969	0.024527783			
	30	0	0.008095566	0.009054734	0.010902217			
		0.5	0.008095108	0.009054249	0.010901727			
		1	0.00809465	0.009053764	0.010901237			

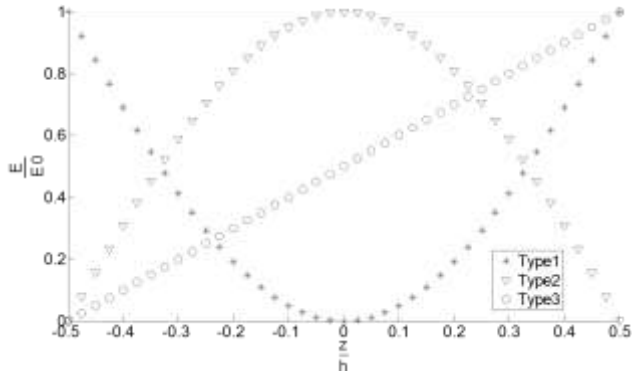


Fig. 3 Young modulus against the distance from the beam axis for three types of porosity distributions

$$v(z) = v_0 \left\{ \left[ e_1 \left( \frac{z}{h} + \frac{1}{2} \right) \right] \right\} \tag{27}$$

The other parameters are the same as described in Type 1 porosity distribution. In Fig. 3 dimensionless Young's modulus against the dimensionless distance from the beam axis for three types of porosity distributions in  $e_1 = 1$  is demonstrated. In Type 1, lower and upper layer of the beam have the maximum Young's modulus. In contrast, the maximum Young's modulus for Type 2 occurs in the middle of beam. Type 3 has an increasing linear distribution its upper layer has the most stiffness.

$$E(z) = E_0 \left\{ \left[ e_1 \left( \frac{z}{h} + \frac{1}{2} \right) \right] \right\} \tag{25}$$

$$G(z) = G_0 \left\{ \left[ e_1 \left( \frac{z}{h} + \frac{1}{2} \right) \right] \right\} \tag{26}$$

Table 3 represents the critical buckling load for three famous volume fraction of carbon nanotube and clamped-free boundary conditions for Configuration 1. As mentioned earlier, Configuration 1 means the core is made of CNTRC and the top and bottom layers are chosen from FRC. Winkler and shear spring constants are considered to be 0.1 and 0.02, respectively. Laminates 1, 2 and 3 (as described earlier) are investigated and it is concluded Laminate 2 has noticeably smaller buckling loads than two other laminates which are really close to each other. Porosity distribution

Table 4 Critical buckling load for three famous volume fraction of carbon nanotube and Clamped-Free boundary conditions for Configuration 2

Configuration 1	L/H	$e_1$	$V_{CNT}$	$\bar{N}_{Cr}$	$V_{CNT}$	$\bar{N}_{Cr}$	$V_{CNT}$	$\bar{N}_{Cr}$
Laminate 1	10	0	0.12	0.074749367	0.17	0.102464767	0.28	0.155847505
		0.5		0.074745087		0.10245955		0.155842081
		1		0.074740807		0.102454332		0.155836657
	20	0	0.018687342	0.025616192	0.038961876			
		0.5	0.018686272	0.025614887	0.03896052			
		1	0.018685202	0.025613583	0.038959164			
30	0	0.008305485	0.011384974	0.017316389				
	0.5	0.00830501	0.011384394	0.017315787				
	1	0.008304534	0.011383815	0.017315184				
Laminate 2	10	0	0.12	2.90454E-05	0.17	4.41188E-05	0.28	5.03052E-05
		0.5		1.98017E-05		3.0078E-05		3.42964E-05
		1		0.000010556		1.60347E-05		1.8284E-05
	20	0	7.26135E-06	1.10297E-05	1.25763E-05			
		0.5	4.95042E-06	7.51949E-06	8.57411E-06			
		1	2.63909E-06	4.00867E-06	4.57101E-06			
30	0	3.22727E-06	4.90209E-06	5.58946E-06				
	0.5	2.20019E-06	3.342E-06	3.81071E-06				
	1	1.17293E-06	1.78163E-06	2.03156E-06				
Laminate 3	10	0	0.12	0.074748775	0.17	0.102464174	0.28	0.155846913
		0.5		0.074744683		0.102459146		0.155841678
		1		0.074740592		0.102454117		0.155836442
	20	0	0.018687194	0.025616044	0.038961728			
		0.5	0.018686171	0.025614786	0.038960419			
		1	0.018685148	0.025613529	0.03895911			
30	0	0.008305419	0.011384908	0.017316324				
	0.5	0.008304965	0.01138435	0.017315742				
	1	0.00830451	0.011383791	0.01731516				

Type 1 is selected and the porosity coefficients are considered to be 0, 0.5 and 1. It is shown that when the porosity coefficient rises, in the described situation, resistance against buckling decreases slightly.

Table 4 demonstrates critical buckling load for similar situations mentioned. The difference is that Configuration 2 is studied. As pointed before, the definition of Configuration 2 is choosing FRC as the core and CNTRC as peripheral layers. The nanocomposite beam is on the Winkler and shear springs with the constants of 0.1 and 0.02, respectively. Comparison between the results of Laminates 1, 2 and 3 showed that buckling loads in Laminate 2 is considerably less than the amounts of two other laminates which are almost the same.

Similarity, porosity distribution Type 1 is selected and the porosity coefficient is considered to be 0, 0.5 and 1. It is shown that when the porosity coefficient rises, in the described situation, buckling resistant reduces smoothly.

Comparing Tables 3 and 4 denotes, when Configuration 2 is selected, the critical buckling load increases about 3 percent in laminate 1 and 3. The amount of increase for laminate 3 is almost 17 percent.

Fig. 4 shows dimensionless critical buckling load versus aspect ratio for two models described in problem section and Figs. 1(b) and (c). As mentioned there, In Model 1, the height of each peripheral layer is one-third of core height. Whereas in Model 2 the height of top or bottom layer is three-fourth of core height. Although the influence of the

core height (which in Model 2 is less than it in Model 1) in the case of  $V_{cnt} = 0.12$  is ignorable, when the amount of volume fraction rises, the differences between two models increases slightly specially in the lower beam aspect ratios.

To study the effect of spring constant factors, critical buckling load is obtained for a range of Winkler constant varying from 0 to 1 and three shear spring constant (0.02, 0.05 and 0.1). Configuration 1 and Laminate 1 are used and CF boundary condition is applied. Porosity coefficient is considered to be 0.5. Volume fraction of carbon nanotube is 0.12 and length is selected to be 10 times of height. It can be observed in Fig. 5 that both of Winkler and shear spring constants, have linear increasing influence on the critical buckling load.

The effect of porosity coefficient on the critical buckling load is shown in Fig. 6 for four boundary conditions. As can be seen, when porosity coefficient and aspect ratio enlarge, the critical buckling loads decline. Also, it can be seen that the critical buckling load for clamped-clamped (CC) boundary conditions is higher than that of other boundary conditions.

To investigate the effect of porosity distribution on critical buckling load, three general types of distribution is considered including Eqs. (19) to (21) for Type 1, Eqs. (23) to (25) for Type 2 and Eqs. (26) to (28) for Type 3. The other situations and parameters are the same as what was described for Fig. 6. It is obvious from Fig. 7, although the

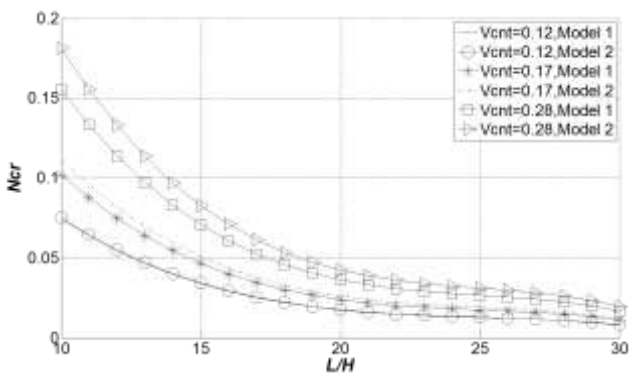


Fig. 4 Critical buckling load against aspect ratio for two models

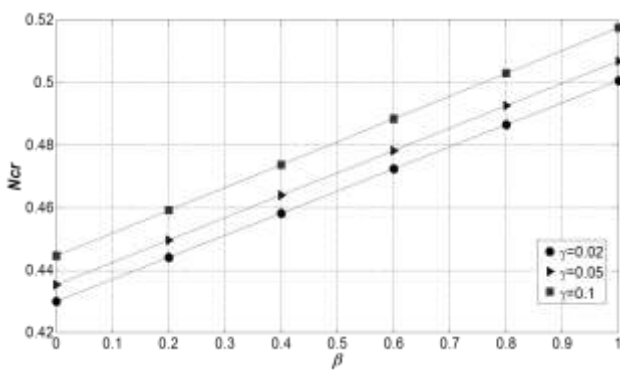


Fig. 5 Critical buckling load against Winkler and shear constants

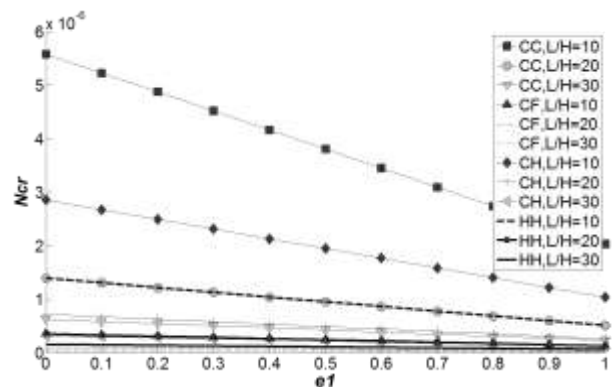


Fig. 6 Critical buckling load against porosity coefficient for four boundary conditions

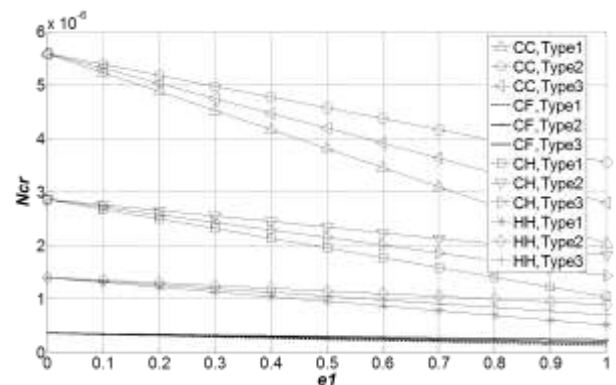


Fig. 7 Critical buckling load for three types of porosity distributions

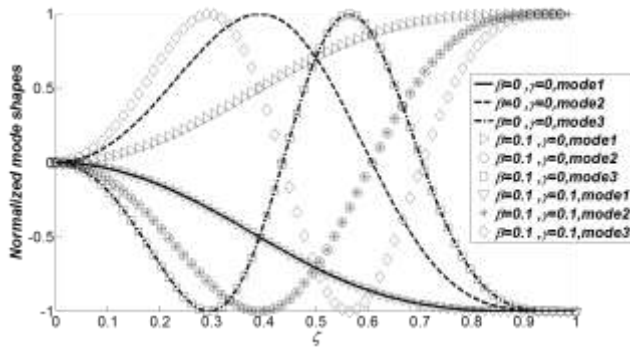


Fig. 8 The first three mode shapes of buckling of sandwich beam

beginning point of three curves is the same, the differences rise by increasing porosity coefficient. It also can be seen that distribution Type 2 gives beam the most resistance against buckling. In contrast, beam with the distribution of porosity Type 1 is the least resistant one. Among four investigated boundary conditions, CC and CF create the most and the least buckling load, respectively.

In Fig. 8, the first three mode shapes of buckling of hybrid beam for four different Winkler ( $\beta$ ) and Pasternak ( $\gamma$ ) constants are presented. In all of them, CF boundary condition is applied and aspect ratio is 10. It is possible to conclude that Winkler spring constant affects first and second mode shapes. While shear spring constant has a slight influence on the third mode shape of buckling.

## 6. Conclusions

In this paper, buckling analysis of sandwich composite beam which is composed of Carbon Nanotube Reinforced Composite (CNTRC) and Fiber Reinforced Composite (FRC) beam in two different configurations, three various laminates and two models using differential quadrature method (DQM) based on Euler-Bernoulli beam theory was studied. Moreover, influences of porosity coefficient and porosity distribution types on critical buckling load were discussed.

Comparing sandwich and CNTRC beam denoted that there is a substantial increase in the critical buckling load by using sandwich beam. In fact, resistance against buckling in sandwich beam is between two to four times more than CNTRC beam. In the other words, although with the increasing of CNT volume fraction, the influence of sandwich beams decreases, it is still significant.

It was concluded that for two configurations 1 and 2, Laminate 1 and 3 (which their results are really close to each other) have remarkably larger buckling loads than laminate 2.

It was also shown using configuration 2, the critical buckling load increases about 3 percent in laminate 1 and 3 compared to the results of configuration 1. The amount of increase in buckling load for laminate 3 reaches about 17 percent.

Comparing two models showed the influence of the core height in the case of lower carbon volume fractions could

be neglected. Even though, when volume fraction of fiber rises, differences increase gently. In addition, the effect is even more in the smaller beam aspect ratios.

Investigating porosity coefficient presented that critical buckling load decreases linearly by increasing porosity coefficient in distribution Type 1. It should be noted the amount of decrease has inverse relationship with the aspect ratio of beam.

Finally it was concluded that in case of assuming porosity distribution Type 2, beam has the most resistance against buckling. Contrary, beam with the distribution of porosity type 1 has the minimum critical buckling load among three other porosity patterns.

## Acknowledgments

The authors would like to thank the referees for their valuable comments. Also, they are thankful to thank the Iranian Nanotechnology Development Committee for their financial support and the University of Kashan for supporting this work by Grant No. 682561/15.

## References

- Alimirzaei, S., Mohammadimehr, M. and Tounsi, A. (2019), "Nonlinear analysis of viscoelastic micro-composite beam with geometrical imperfection using FEM: MSGT electro-magneto-elastic bending, buckling and vibration solutions", *Struct. Eng. Mech., Int. J.*, **71**(5), 485-502.  
<https://doi.org/10.12989/sem.2019.71.5.485>
- Amini, A., Mohammadimehr, M. and Faraji, A.R. (2019), "Active control to reduce the vibration amplitude of the solar honeycomb sandwich panels with CNTRC facesheets using piezoelectric patch sensor and actuator", *Steel Compos. Struct., Int. J.*, **32**(5), 671-686. <https://doi.org/10.12989/scs.2019.32.5.671>
- Anh, V.T.T., Bich, D.H. and Duc, N.D. (2015), "Nonlinear buckling analysis of thin FGM annular spherical shells on elastic foundations under external pressure and thermal loads", *Eur. J. Mech. - A/Solids*, **50**, 28-38.  
<https://doi.org/10.1016/j.euromechsol.2014.10.004>
- Arani, A.J. and Kolahchi, R. (2016), "Buckling analysis of embedded concrete columns armed with Carbonnanotubes", *Comput. Concrete, Int. J.*, **17**(5), 567-578.  
<https://doi.org/10.12989/cac.2016.17.5.567>
- Barati, M.R. and Zenkour, A.M. (2018), "Analysis of postbuckling behavior of general higher-order functionally graded nanoplates with geometrical imperfection considering porosity distributions", *Mech. Adv. Mater. Struct.*, **26**(12), 1081-1088.  
<https://doi.org/10.1080/15376494.2018.1430280>
- Chemi, A., Zidour, M., Heireche, H., Rakrak, K. and Bousahla, A.A. (2018), "Critical buckling load of chiral double-walled carbon nanotubes embedded in an elastic medium", *Mech. Compos. Mater.*, **53**(6), 827-836.  
<https://doi.org/10.1007/s11029-018-9708-x>
- Chen, D., Yang, J. and Kitipornchai, S. (2015), "Elastic buckling and static bending of shear deformable functionally graded porous beam", *Compos. Struct.*, **133**, 54-61.  
<https://doi.org/10.1016/j.compstruct.2015.07.052>
- Cong, P.H., Chien, T.M., Khoa, N.D. and Duc, N.D. (2018), "Nonlinear thermo-mechanical buckling and post-buckling response of porous FGM plates using Reddy's HSDT", *J. Aerosp. Sci. Technol.*, **77**, 419-428.  
<https://doi.org/10.1016/j.ast.2018.03.020>

- Duc, N.D. (2014), "Nonlinear static and dynamic stability of functionally graded plates and shells", Vietnam National University Press. Hanoi, Vietnam.
- Duc, N.D. (2016), "Nonlinear thermal dynamic analysis of eccentrically stiffened S-FGM circular cylindrical shells surrounded on elastic foundations using the Reddy's third-order shear deformation shell theory", *J. Eur. J. Mech. – A/Solids*, **58**, 10-30. <https://doi.org/10.1016/j.euromechsol.2016.01.004>
- Duc, N.D., Bich, D.H. and Cong, P.H. (2016), "Nonlinear thermal dynamic response of shear deformable FGM plates on elastic foundations", *J. Thermal Stresses*, **39**(3), 278-297.
- Duc, N.D., Nguyen, P.D. and Khoa, N.D. (2017a), "Nonlinear dynamic analysis and vibration of eccentrically stiffened S-FGM elliptical cylindrical shells surrounded on elastic foundations in thermal environments", *Thin-wall. Struct.*, **117**, 178-189. <https://doi.org/10.1016/j.tws.2017.04.013>
- Duc, N.D., Tuan, N.D., Tran, P. and Quan, T.Q. (2017b), "Nonlinear dynamic response and vibration of imperfect shear deformable functionally graded plates subjected to blast and thermal loads", *J. Mech. Adv. Mater. Struct.*, **24**(4), 318-329. <https://doi.org/10.1080/15376494.2016.1142024>
- Duc, N.D., Seung-Eock, K. and Chan, D.Q. (2018a), "Thermal buckling analysis of FGM sandwich truncated conical shells reinforced by FGM stiffeners resting on elastic foundations using FSDT", *J. Thermal Stresses*, **41**(3), 331-365. <https://doi.org/10.1080/01495739.2017.1398623>
- Duc, N.D., Quang, V.D., Nguyen, P.D. and Chien, T.M. (2018b), "Nonlinear dynamic response of FGM porous plates on elastic foundation subjected to thermal and mechanical loads using the first order shear deformation theory", *J. Appl. Computat. Mech.*, **4**(4), 245-259. <https://doi.org/10.22055/JACM.2018.23219.1151>
- Esawi, A.M. and Farag, M.M. (2007), "Carbon nanotube reinforced composites: Potential and current challenges", *Mater. Des.*, **28**(9), 2394-2401. <https://doi.org/10.1016/j.matdes.2006.09.022>
- Ghorbanpour Arani, A., Roustavi Navi, B. and Mohammadimehr, M. (2016), "Surface stress and agglomeration effects on nonlocal biaxial buckling polymeric nanocomposite plate reinforced by CNT using various approaches", *Adv. Compos. Mater.*, **25**(5), 423-441. <https://doi.org/10.1080/09243046.2015.1052189>
- Gui, X., Li, H., Zhang, L., Jia, Y., Liu, L., Li, Z., Wei, J., Wang, K., Zhu, H., Tang, Z. and Wu, D. (2011), "A facile route to isotropic conductive nanocomposites by direct polymer infiltration of carbon nanotube sponges", *ACS Nano*, **5**, 4276-4283. <https://doi.org/10.1021/nn201002d>
- Hu, N., Fukunaga, H., Lu, C., Kameyama, M. and Yan, B. (2005), "Prediction of elastic properties of carbon nanotube reinforced composites", *Proc. Royal Soc. A*, **461**, 1685-1710. <https://doi.org/10.12989/sem.2019.71.5.485>
- Jabbari, M., Mojahedin, A., Khorshidvand, A.R. and Eslami, M.R. (2013), "Buckling analysis of a functionally graded thin circular plate made of saturated porous materials", *J. Eng. Mech.*, **140**(2), 287-295. [https://doi.org/10.1061/\(ASCE\)EM.1943-7889.0000663](https://doi.org/10.1061/(ASCE)EM.1943-7889.0000663)
- Jabbari, M., Hashemitaheri, M., Mojahedin, A. and Eslami, M.R. (2014), "Thermal buckling analysis of functionally graded thin circular plate made of saturated porous materials", *J. Therm. Stresses*, **37**(2), 202-220. <https://doi.org/10.1080/01495739.2013.839768>
- Jabbari, M., Rezaei, M. and Mojahedin, A. (2016), "Mechanical Buckling of FG Saturated Porous Rectangular Plate with Piezoelectric Actuators", *Iran. J. Mech. Eng.*, **17**(2), 45-65.
- Kobayashi, Y., Nakazawa, H., Maeda, T., Yasuda, Y. and Morita, T. (2017), "Synthesis of metallic copper nanoparticles and metal-metal bonding process using them", *Adv. Nano Res., Int. J.*, **5**(4), 359-372. <https://doi.org/10.12989/anr.2017.5.4.359>
- Kumar, B.R. (2018), "Investigation on mechanical vibration of double-walled Carbon nanotubes with inter-tube Van der Waals forces", *Adv. Nano Res., Int. J.*, **6**(2), 135-145. <https://doi.org/10.12989/anr.2018.6.2.135>
- Kumar, P. and Srinivas, J. (2017), "Free vibration, bending and buckling of a FG-CNT reinforced composite beam: Comparative analysis with hybrid laminated composite beam", *Multidiscipl. Model. Mater. Struct.*, **13**(4), 590-611. <https://doi.org/10.1108/MMMS-05-2017-0032>
- Lanhe, W. (2004), "Thermal buckling of a simply supported moderately thick rectangular FGM plate", *Compos. Struct.*, **64**, 211-218. <https://doi.org/10.1016/j.compstruct.2003.08.004>
- Low, S. and Shon, Y.S. (2018), "Molecular interactions between pre-formed metal nanoparticles and graphene families", *Adv. Nano Res., Int. J.*, **6**(4), 357-375. <https://doi.org/10.12989/anr.2018.6.4.357>
- Magnucka-Blandzi, E. (2008), "Axisymmetrical deflection and buckling of circular porous-cellular plate", *Thin-wall. Struct.*, **46**, 333-337. <https://doi.org/10.1016/j.tws.2007.06.006>
- Magnucka-Blandzi, E. (2009), "Dynamic stability of a metal foam circular plate", *J. Theor Appl. Mech.*, **47**(2), 421-433.
- Magnucki, K., and Stasiewicz, P. (2004), "Elastic buckling of a porous beam", *J. Theor Appl. Mech.*, **42**(4), 859-868.
- Magnucki, K., Malinowski, M. and Kasprzak, J. (2006), "Bending and buckling of a rectangular porous plate", *Steel Compos. Struct., Int. J.*, **6**(4), 319-333. <https://doi.org/10.12989/scs.2006.6.4.319>
- Mohammadi, M., Saidi, A.R. and Jomehzadeh, E. (2010), "A novel analytical approach for the buckling analysis of moderately thick functionally graded rectangular plates with two simply-supported opposite edges", *Mech. Eng. Sci.*, **224**, 1831-1841. <https://doi.org/10.1243/09544062JMES1804>
- Mohammadimehr, M. and Alimirzaei, S. (2016), "Nonlinear static and vibration analysis of Euler-Bernoulli composite beam model reinforced by FG-SWCNT with initial geometrical imperfection using FEM", *Struct. Eng. Mech.*, **59**(3), 431-454. <https://doi.org/10.12989/sem.2016.59.3.431>
- Mohammadimehr, M. and Mohammadi Hooyeh, H. (2018), "Vibration analysis of magneto-electro-elastic timoshenko micro beam using surface stress effect and modified strain gradient theory under moving nano-particle", *J. Solid Mech.*, **10**(1), 1-22.
- Mohammadimehr, M. and Shahedi, S. (2017), "High-order buckling and free vibration analysis of two types sandwich beam including AL or PVC-foam flexible core and CNTs reinforced nanocomposite face sheets using GDQM", *Compos. Part B*, **108**, 91-107. <https://doi.org/10.1016/j.compositesb.2016.09.040>
- Mohammadimehr, M., Saidi, A.R., Arani, A.G., Arefmanesh, A. and Han, Q. (2010), "Torsional buckling of a DWCNT embedded on winkler and pasternak foundations using nonlocal theory", *J. Mech. Sci. Technol.*, **24**(6), 1289-1299. <https://doi.org/10.1007/s12206-010-0331-6>
- Mohammadimehr, M., Shahedi, S. and Roustavi Navi, B. (2017), "Nonlinear vibration analysis of FG-CNTRC sandwich Timoshenko beam based on modified couple stress theory subjected to longitudinal magnetic field using generalized differential quadrature method", *Proceedings of the Institution of Mechanical Engineers, Part C: J. Mech. Eng. Sci.*, **231**(20), 3866-3885. <https://doi.org/10.1177/0954406216653622>
- Mohammadimehr, M., Okhravi, S.V. and Akhavan Alavi, S.M. (2018), "Free vibration analysis of magneto-electro-elastic cylindrical composite panel reinforced by various distributions of CNTs with considering open and closed circuits boundary conditions based on FSDT", *J. Vib. Control*, **24**(8), 1551-1569. <https://doi.org/10.1177/1077546316664022>
- Mohammadimehr, M., Afshari, H., Salemi, M., Torabi, K. and Mehrabi, M. (2019), "Free vibration and buckling analyses of functionally graded annular thin sector plate in-plane loads using

- GDQM”, *Struct. Eng. Mech., Int. J.*, **71**(5), 525-544.  
<https://doi.org/10.12989/sem.2019.71.5.525>
- Montemurro, M., Vincenti, A. and Vannucci, P. (2012), “Design of the elastic properties of laminates with a minimum number of plies”, *Mech. Compos. Mater.*, **48**(4), 369-390.  
<https://doi.org/10.1007/s11029-012-9284-4>
- Rostami, R., Mohammadimehr, M. and Rahaghi, M.I. (2019), “Dynamic stability and nonlinear vibration of rotating sandwich cylindrical shell with considering FG core integrated with sensor and actuator”, *Steel Compos. Struct., Int. J.*, **32**(2), 225-237.  
<https://doi.org/10.12989/scs.2019.32.2.225>
- Shahedi, S. and Mohammadimehr, M. (2019), “Vibration analysis of rotating fully-bonded and delaminated sandwich beam with CNTRC face sheets and AL-foam flexible core in thermal and moisture environments”, *Mech. Based Des. Struct. Mach.*, 1-31.  
<https://doi.org/10.1080/15397734.2019.1646661>
- Shariat, B.S. and Eslami, M.R. (2007), “Buckling of thick functionally graded plates under mechanical and thermal loads”, *Compos. Struct.*, **78**(3), 433-439.  
<https://doi.org/10.1016/j.compstruct.2005.11.001>
- Shen, H.S. and Zhang, C.L. (2010), “Thermal buckling and postbuckling behavior of functionally graded carbon nanotube-reinforced composite plates”, *Mater. Design*, **31**(7), 3403-3411.  
<https://doi.org/10.1016/j.matdes.2010.01.048>
- Sudheer, M., Pradyoth, K.R. and Somayaji, S. (2015), “Analytical and Numerical Validation of Epoxy/Glass Structural Composites for Elastic Models”, *Am. J. Mater. Sci.*, **5**(3C), 162-168.  
<https://doi.org/10.5923/c.materials.201502.32>
- Tang, H., Li, L. and Hu, Y. (2018), “Buckling analysis of two-directionally porous beam”, *Aerosp. Sci. Technol.*, **78**, 471-479.  
<https://doi.org/10.1016/j.ast.2018.04.045>
- Tayeb Bensattalah, Khaled Bouakkaz, Mohamed Zidour and Tahar Hassaine Daouadji. (2018), “Critical buckling loads of Carbon nanotube embedded in Kerr’s medium”, *Adv. Nano Res., Int. J.*, **6**(4), 339-356. <https://doi.org/10.12989/anr.2018.6.4.339>
- Thostenson, E.T., Ren, Z. and Chou, T.W. (2001), “Advances in the science and technology of carbon nanotubes and their composites: A review”, *Compos. Sci. Technol.*, **61**(13), 1899-1912. [https://doi.org/10.1016/S0266-3538\(01\)00094-X](https://doi.org/10.1016/S0266-3538(01)00094-X)
- Tornabene, F., Fantuzzi, N., Ubertini, F. and Viola, E. (2015), “Strong formulation finite element method based on differential quadrature: a survey”, *Appl. Mech. Rev.*, **67**(2), 020801.  
<https://doi.org/10.1115/1.4028859>
- Wattanasakulpong, N. and Ungbhakorn, V. (2013), “Analytical solutions for bending, buckling and vibration responses of carbon nanotube-reinforced composite beams resting on elastic foundation”, *Computat. Mater. Sci.*, **71**, 201-208.  
<https://doi.org/10.1016/j.commatsci.2013.01.028>
- Wu, H., Kitipornchai, S. and Yang, J. (2015), “Free vibration and buckling analysis of sandwich beams with functionally graded carbon nanotube-reinforced composite face sheets”, *Int. J. Str. Stab. Dyn.*, **15**(7), 1540011.  
<https://doi.org/10.1142/S0219455415400118>
- Yas, M.H. and Samadi, N. (2012), “Free vibrations and buckling analysis of carbon nanotube-reinforced composite”, *Int. J. Press. Vessels Pip.*, **98**, 119-128.  
<https://doi.org/10.1016/j.ijpvp.2012.07.012>
- Zghal, S., Frikha, A. and Dammak, F. (2017), “Static analysis of functionally graded carbon nanotube-reinforced plate and shell”, *Compos. Struct.*, **176**, 1107-1123.  
<https://doi.org/10.1016/j.compstruct.2017.06.015>